# Agarose-Dextran Gels as Synthetic Analogs of Glomerular Basement Membrane: Water Permeability

Jeffrey A. White* and William M. Deen*,†

*Department of Chemical Engineering and †Division of Bioengineering and Environmental Health, Massachusetts Institute of Technology, Cambridge, Massachusetts 02139 USA

ABSTRACT Novel agarose–dextran hydrogels were synthesized and their suitability as experimental models of glomerular basement membrane was examined by measuring their Darcy (hydraulic) permeabilities ($\kappa$). Immobilization of large dextran molecules in agarose was achieved by electron beam irradiation. Composite gels were made with agarose volume fractions ($\phi_a$) of 0.04 or 0.08 and dextran volume fractions ($\phi_d$) ranging from 0 to 0.02 (fiber volume/gel volume), using either of two dextran molecular weights (500 or 2000). At either agarose concentration and for either size of dextran, $\kappa$ decreased markedly as the amount of dextran was increased. Statistically significant deviations from the value of $\kappa$ for pure agarose were obtained for remarkably small volume fractions of dextran: $\phi_d \geq 0.0003$ for $\phi_a = 0.04$ and $\phi_d \geq 0.001$ for $\phi_a = 0.08$. The Darcy permeabilities were much more sensitive to $\phi_d$ than to $\phi_a$, and were as much as 26 times smaller than those of pure agarose. Although $\phi_d$ was an important variable, dextran molecular weight was not. The effects of dextran addition on $\kappa$ were described fairly well using simple structural idealizations. At high agarose concentrations, the dextran chains behaved as fine fibers interspersed among coarse agarose fibrils, whereas, at low concentrations, the dextran molecules began to resemble spherical obstacles embedded in agarose gels. The ability to achieve physiologically relevant Darcy permeabilities with these materials (as low as 1.6 $nm^2$) makes them an attractive experimental model for glomerular basement membrane and possibly other extracellular matrices.

## INTRODUCTION

Pressure-driven flow through extracellular matrices is important in the normal function or pathophysiology of a variety of tissues, including cartilage (Treppo et al., 2000), arterial intima (Baldwin and Wilson, 1993), juxtacanalicular tissue of the eye (Johnson et al., 1992), and tumor interstitium (Netti et al., 2000). Of particular interest to our laboratory is water flow through the glomerular basement membrane (GBM). Flow through that structure is crucial for renal function, in that the ultrafiltration of blood across the walls of glomerular capillaries, which are composed of a layer of fenestrated endothelial cells, the GBM, and a layer of epithelial foot processes, is the first step in urine formation. Two hallmarks of chronic kidney disease are progressive reductions in the glomerular filtration rate of water, and increases in the amounts of protein that are filtered and appear in urine (Blouch et al., 1997; Deen et al., 2001). Inasmuch as the GBM significantly influences both the water-filtration capacity of glomeruli and their ability to selectively retain proteins or other macromolecules in the circulation, there is considerable motivation to measure and explain its transport properties.

The isolation of GBM from rats or other experimental animals, using dissection, sieving to collect whole glomeruli, and detergent lysis to remove cells, has made it possible to measure its hydraulic and macromolecular permeabilities in vitro (Robinson and Walton, 1987; Walton et al., 1992; Daniels et al., 1992, 1993; Edwards et al., 1997; Bolton et al., 1998). Such studies provide the foundation for our current understanding of the contribution of the GBM to the overall permeability properties of the glomerular capillary wall (Deen et al., 2001). However, they yield little insight into the relationship between the functional properties and macromolecular structure of GBM, because it has not been possible to systematically vary (or even fully quantify) the composition of isolated GBM. Moreover, technical limitations have precluded making independent measurements of diffusive and convective hindrance factors for proteins or other macromolecules using the same GBM preparation. The ability to create membranes of desired dimensions and composition has made it attractive to investigate polymeric hydrogels as experimental models. For example, poly(glyceryl methacrylate) gels have been proposed as synthetic analogs of GBM (Leung and Robinson, 1992).

In considering what a synthetic hydrogel should mimic, we note that GBM consists mainly of collagen IV, laminin, and glycosaminoglycans (GAGs) such as heparan sulfate (Yurchenco and Schittny, 1990), and that approximately 90% of its volume is water (Robinson and Walton, 1987; Comper et al. 1993). Collagen IV and laminin have been shown to self-assemble into three-dimensional networks, and are thought to form primary and secondary frameworks in the GBM. Micrographs of collagen IV networks formed in vitro show fibrils ~1.5–6 nm thick (Yurchenco and Ruben, 1988; Yurchenco and Schittny, 1990), whereas those of laminin networks show fibrils ~4 nm thick (Yurchenco et al., 1992). Both fibril sizes are comparable to

*Submitted June 18, 2001, and accepted for publication January 2, 2002.*

Address reprint requests to William M. Deen, Dept. of Chemical Engineering, 66-572, Massachusetts Institute of Technology, 77 Massachusetts Ave., Cambridge, MA 02139. Tel.: 617-253-4535; Fax: 617-258-8224; E-mail: wmdeen@mit.edu



0006-3495/02/04/2081/09 $2.00

typical thicknesses seen in micrographs of GBM (6–8 nm; Bolton and Deen, 2002), suggesting that it is these protein networks (and not the GAGs) that are visualized. Heparan sulfate is an extended, flexible chain of ~1 nm in diameter (Dea et al., 1973). Unlike collagen IV and laminin, heparan sulfate does not appear to form its own network; instead, it attaches to the collagen IV network through disulfide bonds (Parthasarathy and Spiro, 1981). Thus, GBM may be viewed as consisting of at least two types of fibers (coarse and fine), which together comprise about 10% of its volume.

The representation of GBM as a composite gel containing two types of fibers is supported by analyses of its permeability properties measured in vitro (Edwards et al., 1997; Bolton and Deen, 2002). It was found that theories based on a uniform population of fibers were incapable of reconciling the measured hydraulic (or Darcy) permeability, the reported GBM solids content, and the fiber radii observed in micrographs. Only when a substantial number of small-diameter fibers were introduced in the calculations was it possible to account for the relatively low Darcy permeability of GBM (1–2 $nm^2$). Likewise, it was found that a one-fiber representation did not adequately explain the sieving coefficients measured for neutral, spherical test solutes (Ficoll) of various sizes across isolated GBM (Bolton and Deen, 2002). Thus, a mixture of fiber types is suggested both by the biopolymers present and by the known permeability properties.

Agarose gels are an attractive starting point for creating an experimental model of the GBM, because they contain fibrils with diameters of ~4 nm, roughly comparable to those of the relevant protein networks. They are readily made, and have a cross-linked network of fibrils that is rigid enough to exhibit negligible osmotic shrinkage when they are exposed to concentrated solutions of macromolecules (White and Deen, 2001). Moreover, the water permeability and the hindered diffusion and convection of macromolecules have been relatively well studied in agarose gels (Johnson et al., 1995, 1996; Johnson and Deen, 1996; Kong et al., 1997; Pluen et al., 1999; Johnston and Deen, 1999, 2002). Neutral dextran is a reasonable choice for the second polymeric component, because it too is readily available, and its backbone diameter approximates that of heparan sulfate. Although dextran is uncharged and heparan sulfate is a polyanion, the absence of measurable charge selectivity in the filtration of macromolecules across isolated GBM at physiological ionic strength (Bolton et al., 1998) suggests that this difference is not crucial. Accordingly, the objective of the present study was to synthesize agarose-dextran composite hydrogels and to examine their suitability as experimental models of GBM. Immobilization of dextran in agarose gels was achieved by electron beam irradiation. Darcy permeabilities were measured as a function of the relative amounts of agarose and dextran, and the results compared with predictions from various theories for water flow through fibrous media.

## METHODS

### Materials

Agarose (type VI, high-gelling) and unlabeled and FITC-labeled dextrans with nominal (weight-averaged) molecular weights ($M_w$) of 500 or 2000 were purchased from Sigma Chemicals (St. Louis, MO). Before use, solutions of FITC dextran were ultrafiltered across Biomax membranes (50 kDa nominal molecular mass cutoff, Millipore, Bedford, MA) to verify that the amount of free fluorescein was negligible. Polyester meshes (70 $\mu$m thick, 53% open area), used as supports for the gel membranes, were purchased from Spectrum Laboratories (Houston, TX). The buffer solutions used were 0.01 M sodium phosphate at pH 7, with 0.02% sodium azide added as a bactericide.

### Gel synthesis

Agarose-dextran composite gels were synthesized by preparing agarose gels, equilibrating them with dextran solutions, and using electron-beam irradiation to covalently link the dextran to the agarose fibrils. The variables examined were agarose volume fraction, dextran concentration, and dextran molecular weight. Agarose gels with volume fractions ($\phi_a$) of 0.04, 0.06, or 0.08 were prepared by first dissolving agarose in phosphate buffer at pH 7 in an oven at 95°C. (The volume fraction of agarose is essentially the same as its mass concentration in g/ml.; Johnson et al., 1995.) The solutions were allowed to gel at room temperature. The agarose gels were equilibrated with solutions of 2–15% (w/v) of either size of dextran. Relatively large volumes of buffer (~300 × gel volume) were used to incubate the gels, so that the dextran concentration in the buffer would be constant. To ensure equilibrium, the incubation periods equaled several characteristic diffusion times, $\tau_d$. Values for $\tau_d$, estimated using the data of Key and Sellen (1982) for diffusion of 500 and 2000 kDa dextran in agarose, ranged from ~30 min to 5 hr for a gel thickness of 100 $\mu$m.

Electron-beam irradiation links dextran and agarose by using OH radicals formed by the introduction of electrons into the aqueous phase to abstract hydrogen radicals from both dextran and agarose. When a resulting carbon radical from one chain encounters one from another, a cross-link forms. All results presented here are for samples irradiated for ~1 s at a dosage of 2 Mrad, at the High Voltage Research Laboratory at Massachusetts Institute of Technology. In preliminary experiments, several samples (with and without dextran) were irradiated at doses ranging from 1 to 4 Mrad. Within that range, there was no significant effect of dosage on the measured water permeabilities.

### Dextran concentrations in gels

FITC-dextran was used to quantify the amounts of dextran immobilized in the gels. The final dextran concentration in the composite gel ($C_d$) is related to that in the equilibrating buffer ($C_b$) by

$$C_d = \eta \Phi C_b, \quad (1)$$

where $\Phi$ is the equilibrium partition coefficient, and $\eta$ is the immobilization efficiency. The partition coefficient is the concentration of soluble dextran in the gel (based on total gel volume) divided by that in the external solution, before irradiation; the immobilization efficiency is the fraction of the soluble dextran that ultimately remained in the gel. Values of $\Phi$ measured under the conditions of interest are reported elsewhere (White and Deen, 2001), along with a theory that describes the effects of gel concentration, polymer molecular weight, polymer concentration, and other parameters on the partitioning of linear polymers in gels. To measure

$\eta$, composite gels containing agarose and FITC-dextran were synthesized. Gel samples of known volume ($V_g \cong 0.03$ ml) were irradiated, rinsed for 2–3 min, and placed in 10 ml dextran-free buffer for times greatly exceeding $\tau_d$. The relatively large volume of buffer ensured that the dextran mass in the buffer at equilibrium closely approximated that of mobile dextran initially in the gel. Thus, the mass of dextran lost from the gel ($m_d$) was calculated from the product of the final buffer volume and fluorescence, allowing the efficiency to be calculated as

$$\eta = 1 - \frac{m_d}{\Phi C_b V_g}. \quad (2)$$

Immobilized dextran concentrations were converted to volume fractions ($\phi_d$) using $\phi_d = \hat{V}_d C_d$, where $\hat{V}_d = 0.61$ ml/g is the specific volume of dextran (Bohrer et al., 1979). This volume fraction was interpreted as the solid volume of dextran chains (or fibers) divided by the total gel volume, and is the one that appears in most theories for flow through fiber matrices. Another volume fraction (based on the hydrodynamic radius of dextran coils in solution) is discussed later.

## Water permeability

For measurements of the Darcy permeability, agarose gels were cast onto polyester mesh supports as done previously (Johnson and Deen, 1996). After rinsing and blotting, the membranes were equilibrated with dextran solutions and irradiated, as described above. Before use, each membrane was stored at 4°C for a sufficient time to allow any mobile dextran to diffuse from the gel. The hydraulic permeability was determined by placing the membrane in a 3-ml ultrafiltration cell (Amicon, Beverly, MA) and measuring the filtration rate as a function of the applied pressure. The volumetric filtration rate ($Q$) was calculated from the time needed for 0.5 ml buffer to pass through the membrane. To ensure that the membrane had adjusted to changes in the applied pressure, data were not used until two consecutive collection times were identical. Three values of the transmembrane pressure difference ($\Delta P$) were used: 6.7, 13.3, and 20 kPa. Membrane thicknesses were determined afterwards using a micrometer, with the membrane gently confined between glass plates of known thickness; typical membrane thicknesses were 70–90 $\mu$m.

For an isotropic material, the Darcy permeability ($\kappa$), local filtrate velocity ($\mathbf{v}$), and pressure gradient ($\nabla P$) are related by

$$\mathbf{v} = -\frac{\kappa}{\mu}\nabla P. \quad (3)$$

Application of this to a mesh-supported membrane, with $\nabla \cdot \mathbf{v} = 0$ to ensure conservation of mass, gives

$$\kappa = \frac{\mu Q \delta}{\beta A \Delta P}, \quad (4)$$

where $A$ is the exposed area, $\delta$ the membrane thickness, and $\beta$ a correction factor ($\leq 1$) that accounts for the barrier effect of the mesh. The value of $\beta$ is dependent on membrane thickness; for the membranes used here, it was calculated that $\beta = 0.53$ (Johnson and Deen, 1996). The Darcy permeabilities computed from Eq. 4 were found to be insensitive to $\Delta P$. Variations in $\kappa$ were typically $<5\%$ over the range of pressures used, with no clear trend. Consequently, all results are reported as the average $\kappa$ at the three experimental pressures.

## RESULTS

Figure 1 shows the effects of electron beam irradiation on the Darcy permeability of pure agarose ($\kappa_a$). Values for

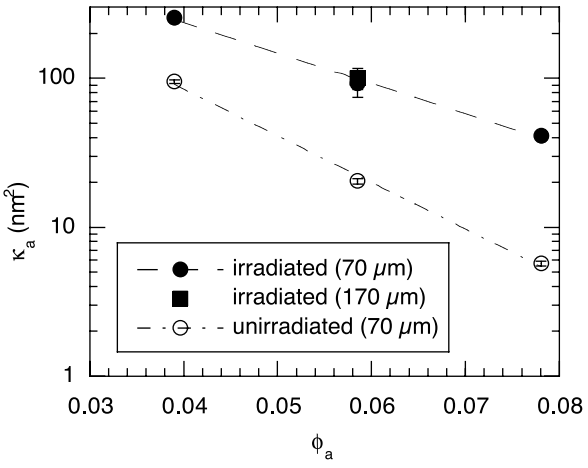


FIGURE 1 Effects of agarose volume fraction ($\phi_a$), electron beam irradiation, and sample thickness on the Darcy permeability of pure agarose ($\kappa_a$). The data for unirradiated gels are from Johnston and Deen (1999). Sample thicknesses are indicated in the legend. The error bars in this and subsequent figures represent one standard deviation.

irradiated gels in the present study are compared with previous results for unirradiated gels (Johnston and Deen, 1999), at various volume fractions of agarose ($\phi_a$). Also shown is a comparison of values obtained at $\phi_a = 0.06$ for irradiated gels of different thickness. The decline in $\kappa_a$ with increasing $\phi_a$ was qualitatively similar for the irradiated and unirradiated gels, but the irradiated gels had Darcy permeabilities that were 3–6 times higher than their untreated counterparts. As shown by the nearly identical results for membrane thicknesses of 70 and 170 $\mu$m, $\kappa_a$ for the irradiated gels was independent of the sample thickness. That is, the electron beam altered the bulk agarose, not just the surface. Evidently, augmenting the normal physical cross-linking in agarose by irradiation-induced cross-links had the effect of increasing $\kappa_a$. Increases in macromolecular permeability, which are likely to parallel changes in $\kappa$, have been observed previously following chemical cross-linking of GBM (Walton et al., 1992) or Matrigel, a gelatinous material extracted from Engelbreth–Holm–Swarm mouse tumors (Boyd-White and Williams, 1996).

The immobilization efficiencies for dextran ($\eta$) in 4% and 8% agarose gels are shown in Figs. 2 and 3, respectively. Both plots show $\eta$ for 500 and 2000-kDa dextrans as a function of the dextran volume fraction ($\phi_d$). At the lower agarose concentration the efficiencies ranged from 0.05 to 0.65, depending on the dextran concentration and molecular weight ($M_w$) (Fig. 2). In this case $\eta$ was proportional to $\phi_d$, the slope decreasing with increasing $M_w$. In contrast, at the higher agarose concentration, there was no apparent dependence of $\eta$ on $\phi_d$ or $M_w$, the efficiencies scattering about a mean value of 0.53 (Fig. 3). The dependence of $\eta$ on $\phi_d$ in 4% agarose suggests that the formation of dextran–dextran bonds facilitated the attachment of dextran to agarose. This may be related to the fact that the average spacing between

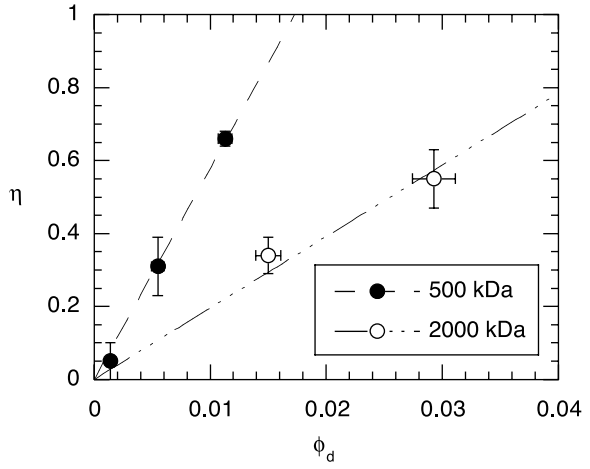


FIGURE 2 Effects of dextran volume fraction ($\phi_d$) and molecular mass on the dextran immobilization efficiency ($\eta$) in 4% agarose gels ($\phi_a = 0.04$).

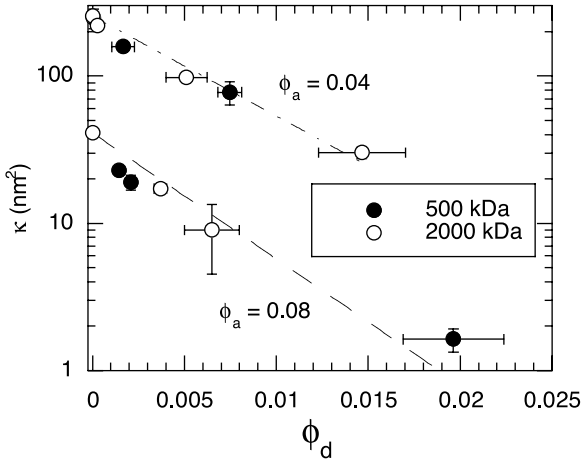


FIGURE 4 Effects of agarose and dextran volume fractions ($\phi_a$ and $\phi_d$, respectively) and dextran molecular mass on the Darcy permeability of composite gels ($\kappa$).

agarose fibrils in 4% gels is comparable to the size of a dextran coil, as will be discussed. In 8% agarose, the inter-fiber spacing is much smaller, and it is likely that dextran and agarose are more fully entangled. This would tend to promote dextran–agarose contacts and, perhaps, make dextran–dextran bonds unimportant for immobilization in the 8% gels. Efficiencies were not measured at irradiation dosages other than 2 Mrad, so that it is not known what dosage (if any) would maximize $\eta$. As stated earlier, preliminary experiments at 1–4 Mrad showed no significant variations in water permeability. Because $\kappa$ in the composite gels was very sensitive to the amount of dextran present (see below), this suggests that $\eta$ is insensitive to electron dosages in this range.

Figure 4 shows values of $\kappa$ measured for agarose–dextran gels, as a function of $\phi_d$. Results are plotted for two agarose volume fractions ($\phi_a = 0.04$ and 0.08) and the two dextran molecular weights. At either agarose concentration and for either size of dextran, $\kappa$ decreased markedly as the amount of dextran was increased. Statistically significant deviations from the value of $\kappa$ for pure agarose (i.e., with $\phi_d = 0$) were obtained for remarkably small volume fractions of dextran: $\phi_d \geq 0.0003$ for $\phi_a = 0.04$ and $\phi_d \geq 0.001$ for $\phi_a = 0.08$. The Darcy permeabilities were much more dependent on the volume fraction of dextran than on that of agarose. For example, the addition of $\phi_d = 0.02$ to an agarose gel with $\phi_a = 0.04$ resulted in a nine-fold reduction in $\kappa$ (Fig. 4), whereas increasing $\phi_a$ from 0.04 to 0.06 resulted in only a two-fold decrease in $\kappa$ (Fig. 1). Although $\phi_d$ was an important variable, $M_w$ was not. As shown by the lines in Fig. 4, the data are well represented by

$$\kappa = \kappa_a \exp(-b\phi_d), \tag{5}$$

where $\kappa_a$ denotes the Darcy permeability of a pure agarose gel at the same $\phi_a$, $b = 156$ for $\phi_a = 0.04$, and $b = 197$ for $\phi_a = 0.08$.

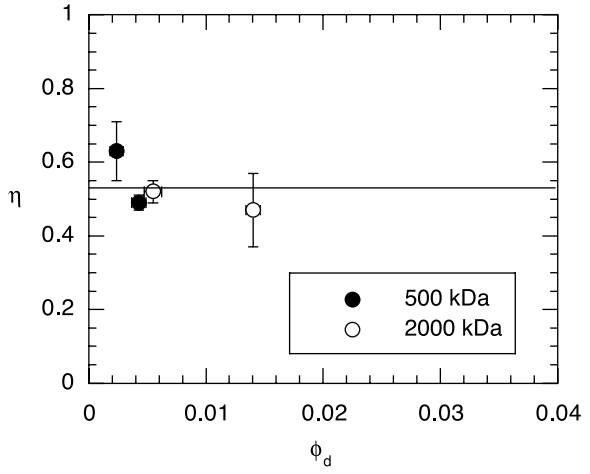


FIGURE 3 Effects of dextran volume fraction ($\phi_d$) and molecular mass on the dextran immobilization efficiency ($\eta$) in 8% agarose gels ($\phi_a = 0.08$).

## DISCUSSION

It was found that incorporating modest amounts of dextran into agarose gels led to large reductions in their Darcy permeability. The ability of small amounts of fine fibers to greatly reduce the Darcy permeability of a fiber matrix is predicted by various hydrodynamic theories (see below), but, to our knowledge, this is the first time this has been demonstrated experimentally using synthetic, composite gels. These findings support the suggestion that the Darcy permeability of GBM is greatly influenced by glycosaminoglycans, and not just the collagen-laminin framework (Edwards et al., 1997; Bolton and Deen, 2002). Indeed, we

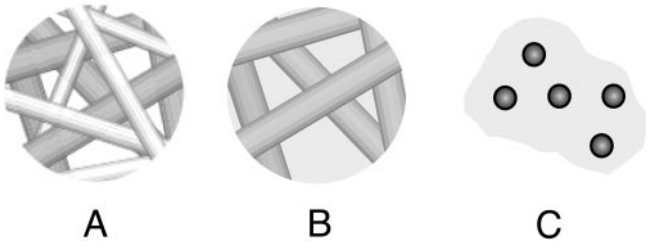


FIGURE 5 Idealized structures of composite gels. (*a*) A matrix of randomly oriented agarose and dextran fibers with water-filled interstices. (*b*) A homogeneous dextran gel with agarose fibers acting as barriers. (*c*) A homogeneous agarose gel with dextran spheres acting as barriers.

were able to create composite gels that quantitatively resemble GBM in certain key respects. Values of $\kappa$ determined for isolated GBM, using modest applied pressures, are typically in the range of 1–2 nm$^2$ (Daniels et al., 1992; Walton et al., 1992; Edwards et al., 1997; Bolton et al., 1998). For our most concentrated gel, corresponding to $\phi_a = 0.08$ and $\phi_d = 0.02$, we found that $\kappa = 1.6$ nm$^2$ (Fig. 4). In addition to the Darcy permeability being in the desired range, the total solid volume of 10% is in good agreement with estimates for GBM (Robinson and Walton, 1987; Comper et al., 1993). Thus, agarose–dextran composite gels are very promising for use in studies designed to elucidate the hindrances to macromolecule diffusion and convection in materials like GBM. Their ease of manipulation should permit a more thorough and controlled examination of macromolecule transport than is possible with isolated GBM.

In the remainder of the paper we examine the ability of existing theories to explain the reductions in Darcy permeability caused by the addition of dextran. Three conceptual representations of the composite gels will be used. In the first, depicted in Fig. 5 *a*, the gel is assumed to consist of a mixture of randomly oriented, cylindrical fibers having two distinct radii, with water-filled interstices between the fibers. The large fibers are agarose fibrils, and the small ones are extended dextran chains. In the second model, Fig. 5 *b*, the composite is represented as a set of discrete fibers embedded within a homogenous gel phase. According to the particular theory used, the fibers are assumed to have either a regular or a random orientation. In this case, the discrete fibers are the agarose fibrils and the continuous phase is a dextran gel. This model should be suitable for systems where there is a large difference between fiber radii and where the small fibers are much more closely spaced than the large ones. The third model, Fig. 5 *c*, consists of spherical obstacles within a homogeneous medium, where the spheres are dextran coils and the continuous phase is an agarose gel.

The Darcy permeability theory that explicitly includes two fiber radii, as in Fig. 5 *a*, is that of Clague and Phillips (1997). They simulated Stokes flow through mixed fibrous media using a numerical version of slender body theory, and examined the validity of various analytical approximations. The result that we apply, which assumes that the radii do not differ greatly, is

$$\frac{1}{\kappa} = \left(\frac{\phi_a}{\phi_a + \phi_d}\right)\frac{1}{\kappa_a(\phi_a)} + \left(\frac{\phi_d}{\phi_a + \phi_d}\right)\frac{1}{\kappa_d(\phi_d)}. \quad (6)$$

The contribution of each fiber type (a or d) to the overall resistivity ($1/\kappa$) is weighted here according to its fractional contribution to the solid volume; $\kappa_i(\phi_i)$ is the Darcy permeability of a medium containing only component *i* at volume fraction $\phi_i$.

One analysis for the situation in Fig. 5 *b* is that of Ethier (1991), who used Brinkman's equation to model flow in a homogeneous gel in which large rods (coarse fibers) were embedded in a cubic lattice. The rather complicated expression that was obtained (given by Eqs. 31, 45, 46, A9, A10 in that paper) is of the form

$$\frac{\kappa}{\kappa_d} = f\left(\phi_a, \frac{\kappa_d}{r_a^2}\right). \quad (7)$$

This relates $\kappa$ for the composite to the Darcy permeability of the continuous phase ($\kappa_d$) and the radius and volume fraction of the coarse fibers ($r_a$ and $\phi_a$). A much simpler expression, valid for randomly oriented coarse fibers, is obtained from the analogy between Darcy flow and steady heat conduction in composite media (Deen, 1998). For a material with impermeable (or nonconducting) cylinders, the result is

$$\frac{\kappa}{\kappa_d} = 1 - \frac{5}{3}\phi_a + O(\phi_a^2). \quad (8)$$

where $\phi_a$ is the volume fraction of the cylinders (agarose fibrils).

To apply either of the first two idealizations, it is necessary to have Darcy permeabilities for pure agarose or pure dextran gels (i.e., $\kappa_a$ or $\kappa_d$). Those may be estimated using a relation given in Clague et al. (2000),

$$\frac{\kappa_i}{r_i^2} = \left[\frac{1}{2}\left(\frac{\pi}{\phi}\right)^{1/2} - 1\right]^2 [0.71407\ \exp(-0.51854\phi_i)], \quad (9)$$

which is a fit to the results of their numerical (lattice-Boltzmann) simulations of Stokes flow through randomly oriented arrays of cylinders of uniform radius. For the solid volume fractions of interest, Eq. 9 agrees well with the semi-empirical expression given by Jackson and James (1986) for random fiber matrices.

In applying Eq. 9 to pure agarose, the fibril radius was taken to be the number-average value reported by Djabourov et al. (1989), or 1.9 nm. The resulting Darcy permeabilities are compared with the measured values for irradiated agarose in Table 1. It is seen that the measured values exceed those predicted from this "one-fiber" theory by factors ranging from 4 to 9, with the agreement being

**TABLE 1 Measured and predicted Darcy permeabilities of agarose gels**

| $\phi_a$ | Measured $\kappa_a$ ($nm^2$) | Predicted $\kappa_a$ ($nm^2$) | |
|---|---|---|---|
| | | One-fiber theory | Two-fiber theory |
| 0.04 | 255 ± 8 | 27 | 31 |
| 0.08 | 41 ± 1 | 10 | 12 |

worse at the lower agarose concentration. Because Djabourov et al. (1989) interpreted their small-angle x-ray scattering data as being represented best by a bimodal distribution of radii, with 87% of the fibers of radius 1.5 nm and 13% of radius 4.5 nm, $\kappa_a$ was computed also by using those parameters in Eq. 6. As shown in Table 1, use of the "two-fiber" theory did not significantly improve the predictions for $\kappa_a$, increasing the values by only ~10%. These discrepancies between theory and data for irradiated agarose gels are much like those noted previously for untreated gels (Clague and Phillips, 1997). The deviations, worsening at lower agarose concentrations, might be related to heterogeneities in the fiber matrix. Chui et al. (1995) using nuclear magnetic resonance and Pernodet et al. (1997) using atomic force microscopy each measured increasingly broad distributions in the effective pore size or fiber spacing with decreasing agarose concentration.

Because the available theories did not yield satisfactory predictions for agarose, experimental values of $\kappa_a$ were used instead of theoretical ones. To apply the model of Ethier (1991), which does not explicitly involve $\kappa_a$, Eq. 7 was rearranged as

$$\kappa = \frac{f(\phi_a, \kappa_d/r_a^2)}{f(\phi_a, \infty)}\,\kappa_a. \tag{10}$$

Because a gel consisting of only coarse fibers corresponds to the limit $\kappa_d \to \infty$ in this model, the form of Eq. 10 ensures that $\kappa = \kappa_a$ in that limit. In factoring out the agarose errors by using experimental values of $\kappa_a$ in Eq. 10 and the other expressions applied to the composite gels, we hoped to better assess the ability of the theories to capture the effects of dextran addition.

The most relevant dextran properties are listed in Table 2. The persistence length ($l_p$) is a measure of the distance along the polymer backbone over which the chain can be considered fairly straight. A least-squares fit of a power-law equation to the data of Garg and Stivala (1978) for dilute dextran solutions yielded $l_p = 1.8$ nm for 500-kDa dextran and $l_p = 1.5$ nm for 2000-kDa dextran. The backbone or fiber radius ($r_d$) was computed as the radius of a cylinder having the same contour length and specific volume as dextran, which gave $r_d = 0.27$ nm (White and Deen, 2001). The Stokes–Einstein radius ($r_s$), which is the radius of a solid sphere that would have the same diffusivity in free solution, was obtained from Nordmeier et al. (1993). It is important to bear in mind the distinction between the dextran fiber radius, which is independent of molecular weight, and the Stokes–Einstein radius, which is a measure of the coil size in solution and therefore increases with molecular weight.

**TABLE 2 Dextran properties**

| $M_w$ (kDa) | $l_p$ (nm) | $r_d$ (nm) | $r_s$ (nm) |
|---|---|---|---|
| 500 | 1.8 | 0.27 | 14 |
| 2000 | 1.5 | 0.27 | 27 |

The remaining length scale that affects the selection of models is the interfiber spacing in agarose. The most commonly used measure of microstructural dimensions in disordered materials is $\sqrt{\kappa}$. As the natural length scale in Darcy's law or Brinkman's equation, this should reflect the order of magnitude of the interfiber spacing. Alternatively, one can estimate a spacing parameter for a random array of fibers by using the probability of finding the nearest fiber axis at a certain distance from an arbitrary point in the material. Integrating the probability density of Ogston (1958) to determine the mean (expected value) of this distance, we obtain $(r_f/2)\sqrt{\pi/\phi}$, where $r_f$ and $\phi$ are the radius and volume fraction, respectively, of the hypothetical fiber array.

Using either the Darcy permeability of 41 $nm^2$ (Table 1) or the formula obtained from the Ogston distribution, the characteristic fiber spacing of 8% agarose gels is estimated as 6 nm. This is much smaller than the hydrodynamic radius of either dextran coil ($r_s = 14$ or 27 nm) and does not greatly exceed the persistence lengths ($l_p = 1.8$ or 1.5 nm). This suggests that, on the length scale of the agarose fiber spacings, dextran molecules entrapped in 8% gels might resemble straight rods, as in Fig. 5 *a*, which motivates the use of Eq. 6. However, given the large (seven-fold) difference between the agarose and dextran fiber radii, the model in Fig. 5 *b* might also be valid, making Eqs. 8 or 10 applicable. Predictions of these models are compared with data for the 8% agarose composites in Fig. 6. Excellent results were obtained with either Eq. 8 or Eq. 10, where the dextran was viewed as part of a homogeneous gel filling the spaces between the agarose fibrils. Eq. 6 was found to be much less satisfactory, yielding values about two-fold higher than those measured. The reason for these large discrepancies is not entirely clear, although it may be recalled that Eq. 6 is expected to be most accurate when the two fiber radii do not differ greatly.

The expressions corresponding to Fig. 5 *b* differ mainly in their predictions for $\phi_d \to 0$, which corresponds to $\kappa_d \to \infty$; Eq. 10 gives a finite value of $\kappa$ but Eq. 8 does not. Using Brinkman's equation to describe flow in the continuous (dextran) phase allows no-slip conditions to be imposed on the fiber surfaces and, in this limit, corresponds to Stokes flow through an array of cylinders (agarose fibrils). Thus, Eq. 10 yields a finite flow resistance even for $\kappa_d \to \infty$.

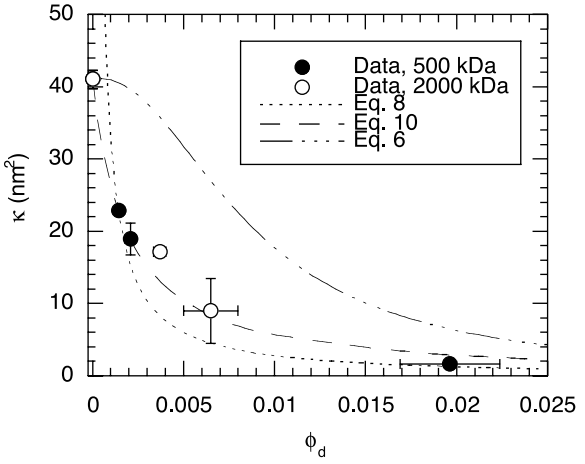


FIGURE 6 Measured and predicted Darcy permeabilities ($\kappa$) of agarose–dextran composites with 8% agarose ($\phi_a = 0.08$). Eq. 6 assumes two discrete types of fibers [Fig. 5 *a*]; Eqs. 8 and 10 assume a homogeneous dextran gel with agarose fibrils acting as barriers [Fig. 5 *b*].

However, when Darcy's law is used for the continuous phase, as assumed in Eq. 8, the overall flow resistance vanishes for $\kappa_d \to \infty$. The fairly similar results obtained from Eqs. 8 and 10 for most values of $\phi_d$ (Fig. 6) indicates that the differing geometric assumptions (cubic lattice versus randomly orientated cylinders) were of only secondary importance. The simplicity of Eq. 8 makes its success particularly impressive.

Figure 7 compares the theories and data for 4% agarose gels. Over most of the dextran concentration range, the measured values of $\kappa$ significantly exceeded those predicted by any of the expressions discussed above (Eqs. 6, 8, or 10). That is, those theories tended to greatly overestimate the

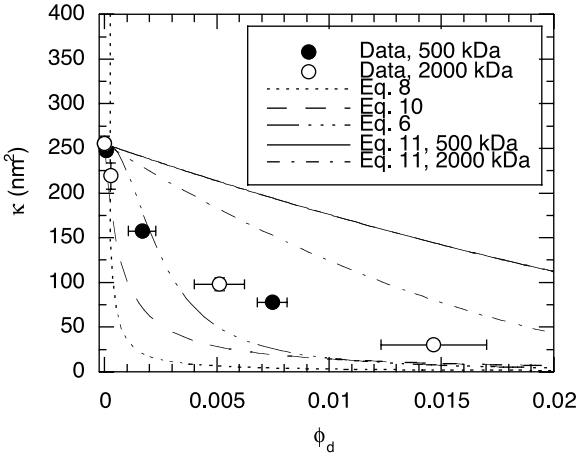


FIGURE 7 Measured and predicted Darcy permeabilities ($\kappa$) of agarose–dextran composites with 4% agarose ($\phi_a = 0.04$). Eq. 6 assumes two discrete types of fibers [Fig. 5 *a*]; Eqs. 8 and 10 assume a homogeneous dextran gel with agarose fibrils acting as barriers [Fig. 5 *b*]; Eq. 11 assumes a homogeneous agarose gel with dextran spheres acting as barriers [Fig. 5 *c*].

effect of adding dextran to a 4% agarose gel. In examining what is different from 8% agarose, we note that the characteristic fiber spacing of 4% gels is estimated as 8–16 nm, depending on the method used. Such spacings are five- to ten-fold larger than the dextran persistence lengths, and begin to approach the hydrodynamic radii of the coils. This suggests that, for dextran in the more dilute agarose gels, a reasonable idealization might be that of unperturbed dextran coils occupying some of the spaces between agarose fibrils. As already noted in connection with Figs. 2 and 3, such a change in the relative length scales may account for the very different trends in immobilization efficiency in 4% and 8% agarose.

The simplest representation of the effect of discrete dextran molecules is Fig. 5 *c*, where spherical dextran coils are assumed to be embedded in a homogeneous agarose gel. In this model, the dextrans were assumed to behave as impermeable spheres of radius $r_s$. One might model flow in this composite by treating the spheres as permeable objects, each characterized by an internal Darcy permeability ($\kappa_s$) that depends on the fraction of solids within a coil. However, a continuum (Darcy) model for flow through a dextran coil would be valid only if the internal chain spacing were much smaller than the coil size; that is, this approach would require that $\sqrt{\kappa_s} \ll r_s$. Assuming that a factor of 10 is sufficient, we would need to have $\sqrt{\kappa_s} < 1.4$ nm for 500 kDa and 2.7 nm for 2000 kDa (Table 2), or $\kappa_s < 2$ and 7 nm$^2$, respectively. Because even the larger of these values of $\kappa_s$ is much smaller than the Darcy permeability of 4% agarose ($\kappa_s/\kappa_a < 7/255 = 0.03$), we conclude that the spheres may as well be modeled as impermeable solids.

The Darcy permeability for this last model was calculated using the effective conductivity derived by Jeffrey (1973) for random suspensions of spheres. For the case of impermeable (nonconducting) particles, that result is

$$\frac{\kappa}{\kappa_a} = 1 - \frac{3}{2}\phi_s + 0.588\phi_s^2, \qquad (11)$$

where $\phi_s$ is the volume fraction of spheres (dextran coils) in the composite gel. A comparison with the numerical results of Bonnecaze and Brady (1991) for poorly conducting particles indicates that Eq. 11 is remarkably accurate even near close packing. Considering the specific volume, molecular mass, and Stokes–Einstein radii of the dextrans, the relationships between the sphere and fiber volume fractions are $\phi_s = 22.7\phi_d$ for 500 kDa and $\phi_s = 40.7\phi_d$ for 2000 kDa. Whereas $\phi_d$ never exceeded 0.02 (Fig. 4), the calculated $\phi_s$ was as large as 0.60. Although this approaches the limit of 0.64 for randomly close-packed spheres of uniform radius (Berryman, 1983), we note that higher values are possible for mixtures of spheres and that the commercial dextrans used were relatively polydisperse (White and Deen, 2001). As shown by the curves in Fig. 7 based on Eq. 11, the sphere model overestimates $\kappa$ for the 4% agarose composites. Also,

it predicts a dependence on molecular mass that was not evident in the data. Nonetheless, the fact that the data are bounded by the fiber and sphere models suggests that flow in the 4% agarose composites may represent a transition between the two types of behavior. It was impractical to test whether the sphere model would become more accurate for lower concentrations of agarose (e.g., 2%), because of the fragility of such dilute gels.

In summary, we synthesized novel agarose–dextran composite gels and characterized their composition and water (Darcy) permeability. Modest amounts of dextran covalently linked to agarose by electron beam irradiation caused very significant reductions in the Darcy permeability, by as much as an order of magnitude. The effects of dextran addition on the Darcy permeability were described fairly well using simple structural idealizations. At high agarose concentrations, the dextran chains behaved as fine fibers interspersed among coarse agarose fibrils, whereas, at low concentrations, the dextran molecules began to resemble spherical obstacles embedded in agarose gels. The ability to achieve physiologically relevant Darcy permeabilities with these materials makes them an attractive experimental model for GBM and possibly other extracellular matrices.

Dr. Edward W. Merrill suggested the use of electron beam irradiation to covalently link dextran to agarose, and Mr. Kenneth A. Wright provided invaluable assistance in exposing the gels to the beam.

This work was supported by grant DK20368 from the National Institutes of Health. J.A.W. is the recipient of a National Science Foundation Graduate Fellowship.

## REFERENCES

Baldwin, A. L., and L. M. Wilson. 1993. Endothelium increases medial hydraulic conductance of aorta, possibly by release of EDRF. *Am. J. Physiol. Heart Circ. Physiol.* 264:H26–H33.

Berryman, J. G. 1983. Random close packing of hard spheres and disks. *Phys. Rev. A.* 27:1053–1061.

Blouch, K., W. M. Deen, J.-P. Fauvel, J. Bialek, G. Derby, and B. D. Myers. 1997. Molecular configuration and glomerular size selectivity in healthy and nephrotic humans. *Am. J. Physiol. Renal Physiol.* 273: F430–F437.

Bohrer, M. P., W. M. Deen, C. R. Robertson, J. L. Troy, and B. M. Brenner. 1979. Influence of molecular configuration on the passage of macromolecules across the glomerular capillary wall. *J. Gen. Physiol.* 74:583–593.

Bolton, G. R., W. M. Deen, and B. S. Daniels. 1998. Assessment of the charge-selectivity of glomerular basement membrane using Ficoll sulfate. *Am. J. Physiol. Renal Physiol.* 274:F889–F896.

Bolton, G. R., and W. M. Deen. 2002. Limitations in the application of fiber-matrix models to glomerular basement membrane. *In* Membrane Transport and Renal Physiology. H. E. Layton and A. M. Weinstein, editors. IMA Volumes in Mathematics and Its Applications Series. Vol. 129. Springer-Verlag, New York. 141–156.

Bonnecaze, R. T., and J. F. Brady. 1991. The effective conductivity of random suspensions of spherical particles. *Proc. R. Soc. Lond. A* 432: 445–465.

Boyd-White, J., and J. C. Williams. 1996. Effect of cross-linking on matrix permeability—a model for AGE-modified basement membranes. *Diabetes.* 45:348–353.

Chui, M. M., R. J. Phillips, and M. J. McCarthy. 1995. Measurement of the porous microstructure of hydrogels by nuclear magnetic resonance. *J. Colloid Interface Sci.* 174:336–344.

Clague, D. S., B. D. Kandhai, R. Zhang, and P. M. A. Sloot. 2000. Hydraulic permeability of (un)bounded fibrous media using the lattice Boltzmann method. *Phys. Rev. E.* 61:616–625.

Clague, D. S., and R. J. Phillips. 1997. A numerical calculation of the hydraulic permeability of three-dimensional disordered fibrous media. *Phys. Fluids.* 9:1562–1572.

Comper, W. D., A. S. N. Lee, M. Tay, and Y. Adal. 1993. Anionic charge concentration of rat-kidney glomeruli and glomerular basement membrane. *Biochem. J.* 289:647–652.

Daniels, B. S., E. B. Hauser, W. M. Deen, and T. H. Hostetter. 1992. Glomerular basement membrane: in vitro studies of water and protein permeability. *Am. J. Physiol. Renal Physiol.* 262:F919–F926.

Daniels, B. S., W. M. Deen, G. Mayer, T. Meyer, and T. H. Hostetter. 1993. Glomerular permeability barrier in the rat: functional assessment by in vitro methods. *J. Clin. Invest.* 92:929–936.

Dea, I. C., M. R. Moorhouse, D. A. Rees, S. Arnott, J. M. Guss, and E. A. Balazs. 1973. Hyaluronic acid. A novel double helical molecule. *Science.* 179:560–562.

Deen, W. M. 1998. Analysis of Transport Phenomena. Oxford University Press, New York. 201.

Deen, W. M., M. J. Lazzara, and B. D. Myers. 2001. Structural determinants of glomerular permeability. *Am. J. Physiol. Renal Physiol*. 281: F579–F596.

Djabourov, M., A. H. Clark, D. W. Rowland, and S. B. Ross-Murphy. 1989. Small-angle x-ray-scattering characterization of agarose sols and gels. *Macromolecules.* 22:180–188.

Edwards, A., B. S. Daniels, and W. M. Deen. 1997. Hindered transport of macromolecules in isolated glomeruli. II. Convection and pressure effects in basement membrane. *Biophys. J.* 72:214–222.

Ethier, C. R. 1991. Flow through mixed fibrous porous materials. *AIChE J.* 37:1227–1236.

Garg, S. K., and S. S. Stivala. 1978. Assessment of branching in polymers from small-angle X-ray scattering (SAXS). *J. Polym. Sci. Polym. Phys. Ed.* 16:1419–1434.

Jackson, G. W., and D. F. James. 1986. The permeability of fibrous porous media. *Can. J. Chem. Eng.* 64:364–374.

Jeffrey, D. J. 1973. Conduction through a random suspension of spheres. *Proc. Roy. Soc. Lond. A.* 335:355–367.

Johnson, E. M., D. A. Berk, R. K. Jain, and W. M. Deen. 1995. Diffusion and partitioning of proteins in charged agarose gels. *Biophys. J.* 68: 1561–1568.

Johnson, E. M., D. A. Berk, R. K. Jain, and W. M. Deen. 1996. Hindered diffusion in agarose gels: test of effective medium model. *Biophys. J.* 70:1017–1026.

Johnson, E. M., and W. M. Deen. Hydraulic permeability of agarose gels. 1996. *AIChE J.* 42:1220–1224.

Johnson, M., A. Shapiro, C. R. Ethier, and R. D. Kamm. 1992. Modulation of outflow resistance by the pores of the inner wall endothelium. *Investig. Ophthalmol. Vis. Sci.* 33:1670–1675.

Johnston, S. T., and W. M. Deen. 1999. Hindered convection of proteins in agarose gels. *J. Membr. Sci.* 153:271–279.

Johnston, S. T., and W. M. Deen. 2002. Hindered convection of Ficoll and proteins in agarose gels. *Ind. Eng. Chem. Res*. 41:340–346.

Key, P. Y., and D. B. Sellen. 1982. A laser light-scattering study of the structure of agarose gels. *J. Polym. Sci. Poly. Phys. Ed.* 20:659–679.

Kong, D. D., T. F. Kosar, S. R. Dungan, and R. J. Phillips. 1997. Diffusion of proteins and nonionic micelles in agarose gels by holographic interferometry. *AIChE J.* 43:25–32.

Leung, B. K.-O., and G. B. Robinson. 1992. The permselectivity of poly(glyceryl methacrylate) membranes—hydrogel analogs of glomerular basement membrane. *Polymer.* 3:3717–3722.

Netti, P. A., D. A. Berk, M. A. Swartz, A. J. Grodzinsky, and R. K. Jain. 2000. Role of extracellular matrix assembly in interstitial transport in solid tumors. *Cancer Res*. 60:2497–2503.

Nordmeier, E., H. Xing, and M. Lechner. 1993. Static and dynamic light-scattering studies of dextran from *Leuconostoc mesenteroides* in the dilute region. *Makromol. Chem.* 194:2923–2937.

Ogston, A. G. 1958. The spaces in a uniform random suspension of fibers. *Trans. Faraday Soc.* 54:1754–1757.

Parthasarathy, N., and R. G. Spiro. 1981. Characterization of the glycosaminoglycan component of the renal glomerular basement membrane and its relationship to the peptide portion. *J. Biol. Chem.* 256:507–513.

Pernodet, M., M. Maaloum, and B. Tinland. 1997. Pore size of agarose gels by atomic force microscopy. *Electrophoresis.* 18:55–58.

Pluen, A., P. A. Netti, R. K. Jain, and D. A. Berk. 1999. Diffusion of macromolecules in agarose gels: comparison of linear and globular configurations. *Biophys. J.* 77:542–552.

Robinson, G. B., and H. A. Walton. 1987. Ultrafiltration through basement membranes. *In* Renal Basement Membranes in Health and Disease. R. G. Price and B. G. Hudson, editors. Academic Press, London. 147–161.

Treppo, S., H. Koepp, E. C. Quan, A. A. Cole, K. E. Kuettner, and A. J. Grodzinsky. 2000. Comparison of biomechanical and biochemical properties of cartilage from human knee and ankle pairs. *J. Orthopaed. Res.* 18:739–748.

Walton, H. A., J. Byrne, and G. B. Robinson. 1992. Studies of the permeation properties of glomerular basement membrane—cross-linking renders glomerular basement membrane permeable to protein. *Biochim. Biophys. Acta.* 1138:173–183.

White, J. A., and W. M. Deen. 2001. Effects of solute concentration on equilibrium partitioning of flexible macromolecules in fibrous membranes and gels. *Macromolecules.* 34:8278–8285.

Yurchenco, P. D., Y. Cheng, and H. Colognato. 1992. Laminin forms an independent network in basement membranes. *J. Cell Biol.* 117: 1119–1133.

Yurchenco, P. D., and J. C. Schittny. 1990. Molecular architecture of basement membranes. *FASEB J.* 4:1577–1590.

Yurchenco, P. D., and G. C. Ruben. 1988. Type-IV collagen lateral associations in the EHS tumor matrix—comparison with amniotic and in vitro networks. *Am. J. Pathol.* 132:278–291.